


## Two- and three-point functions at criticality: Monte Carlo simulations of the three-dimensional $(q + 1)$ -state clock model

Martin Hasenbusch 

*Institut für Theoretische Physik, Universität Heidelberg, Philosophenweg 19, 69120 Heidelberg, Germany*



(Received 19 October 2020; revised 2 December 2020; accepted 3 December 2020; published 21 December 2020)

We simulate the improved  $(q + 1)$ -state clock model on the simple-cubic lattice at the critical point on lattices of a linear size up to  $L = 960$ . We compute operator product expansion coefficients for the three-dimensional  $XY$  universality class. These are compared with highly accurate estimates obtained by using the conformal bootstrap method. We find that the results are consistent.

DOI: [10.1103/PhysRevB.102.224509](https://doi.org/10.1103/PhysRevB.102.224509)

### I. INTRODUCTION

In recent years substantial progress in critical phenomena in three dimensions has been achieved by using the conformal bootstrap (CB) method. For reviews, see, for example, [1,2]. In particular, in the case of the three-dimensional Ising universality class, the results for critical exponents are considerably more accurate than those obtained by other methods [3,4]. Very recently also accurate results for the three-dimensional  $XY$  universality class were provided [5].

In addition to critical exponents, the CB method provides accurate estimates for so called operator product expansion (OPE) coefficients  $\lambda_{ijk}$ . These are defined by the behavior of three-point functions at the critical point. The OPE coefficients are difficult to access by other methods. In the case of the three-dimensional Ising universality class, only recently results have been obtained by using Monte Carlo simulations of lattice models [6–9]. These are far less precise than those obtained by using the CB method. However, the agreement of the results from the lattice and CB method gives further support for the fact that both methods examine the same renormalization group (RG) fixed point.

The functional form of two-point functions of primary operators is fixed by conformal invariance

$$\langle O_1(x_1)O_2(x_2) \rangle = \frac{C_1 \delta_{\Delta_1, \Delta_2}}{|x_1 - x_2|^{2\Delta_1}}, \quad (1)$$

where  $O_i$  is the operator taken at the site  $x_i$ , and  $\Delta_i$  is its scaling dimension.

Also the form of three-point functions is fixed by conformal invariance. Normalizing the operators such that  $C_i = 1$ , Eq. (1), one gets [10]

$$\langle O_1(x_1)O_2(x_2)O_3(x_3) \rangle = \frac{\lambda_{123}}{|x_1 - x_2|^{\Delta_1 + \Delta_2 - \Delta_3} |x_2 - x_3|^{\Delta_2 + \Delta_3 - \Delta_1} |x_3 - x_1|^{\Delta_3 + \Delta_1 - \Delta_2}}, \quad (2)$$

where the OPE coefficients  $\lambda_{123}$  depend on the universality class. For a detailed discussion, see, for example, Ref. [1].

In the present work, we apply the idea of Ref. [9] to the  $XY$  universality class in three dimensions. To this end, we simulate the improved  $O(2)$ -symmetric  $\phi^4$  model and the improved  $(q + 1)$ -state clock model on the simple-cubic lattice at the critical temperature. To reduce the statistical error of the two- and three-point functions, we use a variance reduction method [11,12]. To reduce finite-size effects, large linear lattice sizes  $L$  are considered. In our simulations, we go up to  $L = 960$ . On top of that, an extrapolation to  $L \rightarrow \infty$  is still needed. Our estimates for the OPE coefficients turn out to be consistent with those obtained by using the CB method.

In Table I we summarize results for the scaling dimensions  $\Delta_i$  and the OPE coefficients  $\lambda_{ijk}$  obtained by using the CB method. In the case of the scaling dimensions, we give the most accurate results obtained from Monte Carlo simulations [13–15] of lattice models for comparison. In the case of  $\Delta_s$ , we also give the estimate obtained by analyzing specific-heat data for  ${}^4\text{He}$  near the  $\lambda$ -transition [16–18]. Note that the scaling dimensions are related with the critical exponents that are usually discussed in critical phenomena [19]. In particular, the critical exponent of the correlation length is given by  $\nu = 1/(3 - \Delta_s)$  and the exponent of the correlation function at criticality  $\eta = 2\Delta_\phi - 1$ . The estimate of  $\nu$  obtained by using high temperature (HT) series and Monte Carlo simulations of lattice models [20,21] differs from that obtained from experiments [16–18] by several times the combined error. Recent Monte Carlo studies [13,14] and the CB work [5] confirm the results of Refs. [20,21].

The outline of the paper is the following. In Sec. II we define the models that are simulated and we summarize numerical results, for example for the critical temperature, which are used in our simulations. Next, in Sec. III we define the observables and briefly recall the variance reduction method. In Sec. IV we discuss the simulations and analyze our numerical results. Finally, we conclude and give an outlook.

### II. THE LATTICE MODELS

We performed preliminary simulations by using the  $O(2)$ -symmetric  $\phi^4$  model on the lattice. The final results were

TABLE I. Scaling dimensions and OPE coefficients for the three-dimensional XY universality class. Comparison of conformal bootstrap (CB) results [3,5] with estimates from Monte Carlo (MC) or experiment (EXP). The leading charge 0, 1, and 2 scalars are denoted by  $s$ ,  $\phi$ ,  $t$ , respectively. For a discussion of the meaning of the errors that are quoted, see the references.

Quantity	Method	Value	Ref.
$\Delta_s$	EXP	1.50946(22)	[16–18]
	MC	1.51153(40)	[13]
	MC	1.51122(15)	[14]
	CB	1.51136(22)	[5]
$\Delta_\phi$	CB	1.5117(25)	[3]
	MC	0.51927(24)	[13]
	MC	0.519050(40)	[14]
	CB	0.519088(22)	[5]
$\Delta_t$	CB	0.51926(32)	[3]
	MC	1.2361(11)	[15]
$\lambda_{\phi\phi s}$	CB	1.23629(11)	[5]
	CB	0.687126(27)	[5]
$\lambda_{sss}$	CB	0.68726(65)	[3]
	CB	0.830914(32)	[5]
$\lambda_{ts}$	CB	0.8286(60)	[3]
	CB	1.25213(14)	[5]
$\lambda_{\phi\phi t}$	CB	1.213408(65)	[5]

obtained from simulations of the  $(q+1)$ -state clock model with  $q = 32$ . Note that in the limit  $q \rightarrow \infty$ , the dynamically diluted XY model studied in Refs. [20,21] is reached. Both models have a parameter that can be tuned such that leading corrections to scaling vanish. Models taken at a good approximation of this value are denoted as improved. The idea to study improved models to get better precision on universal quantities goes back to Refs. [22,23]. For a discussion, see, for example, Sec. 2.3 of the review [19].

In the following, we define the models and summarize estimates of the improved models and the inverse critical temperature given in the literature.

### A. The $O(2)$ -symmetric $\phi^4$ model

The  $O(N)$ -symmetric  $\phi^4$  model on the simple-cubic lattice is defined by the reduced Hamiltonian

$$\mathcal{H}_{\phi^4} = -\beta \sum_{\langle xy \rangle} \vec{\phi}_x \cdot \vec{\phi}_y + \sum_x \left[ \vec{\phi}_x^2 + \lambda (\vec{\phi}_x^2 - 1)^2 \right], \quad (3)$$

where  $\vec{\phi}_x \in \mathbb{R}^N$  is the field at the site  $x = (x^{(0)}, x^{(1)}, x^{(2)})$ , where  $x^{(i)} \in \{0, 1, 2, \dots, L_i - 1\}$ . Here we are labeling the components of  $x$  by an upper index. A lower index is used to discriminate different sites on the lattice.  $\langle xy \rangle$  denotes a pair of nearest-neighbor sites on the simple-cubic lattice. In our simulations,  $L_0 = L_1 = L_2 = L$  throughout. In the present work, we consider the case  $N = 2$ .

For the  $O(2)$ -symmetric  $\phi^4$  model on the simple-cubic lattice, the authors of Ref. [21] find for the improved model  $\lambda^* = 2.15(5)$  and  $\beta_c = 0.509\,150\,3(3)[3]$  and  $0.508\,335\,5(3)[4]$  for  $\lambda = 2.1$  and  $2.2$ , respectively. These estimates are obtained by requiring that  $(Z_a/Z_p)^* = 0.3203(1)[3]$ , where  $Z_p$  and  $Z_a$  are the partition functions for a system with periodic boundary

conditions in all directions and antiperiodic in one direction and periodic in the remaining ones, respectively. The superscript  $*$  refers to the fixed point value for the given lattice geometry. The number quoted in parentheses refers to the statistical error obtained in a specific fit, while the number given in square brackets is an estimate of the systematic error. In the case of  $\beta_c$ , the number given in square brackets is the error due to the uncertainty of  $(Z_a/Z_p)^*$ . Here we have reanalyzed unpublished data generated in 2013 for  $\lambda = 2.1$  using the estimates  $(Z_a/Z_p)^* = 0.320\,37(6)$  and  $(\xi_{2\text{nd}}/L)^* = 0.592\,38(7)$  given in Table 3 of Ref. [14] as input. We arrive at

$$\beta_c(\lambda = 2.1) = 0.509\,150\,4(1), \quad (4)$$

where the number quoted in parentheses includes both the statistical as well as the systematic error. We simulate the  $O(2)$ -symmetric  $\phi^4$  model by using a hybrid of local METROPOLIS, local overrelaxation, and single-cluster [24] updates. For a discussion of this algorithm, see, for example, Appendix A of Ref. [15].

### B. The $(q+1)$ -state clock model

The model can be viewed as a generalization of the  $q$ -state clock model. The field  $\vec{s}_x$  at the site  $x = (x^{(0)}, x^{(1)}, x^{(2)})$ , where  $x^{(i)} \in \{0, 1, 2, \dots, L_i - 1\}$ , might assume one of the following values:

$$\vec{s}_x \in \{(0, 0), (\cos(2\pi m/q), \sin(2\pi m/q))\}, \quad (5)$$

where  $m \in \{1, \dots, q\}$ . In our simulations, we take  $L_0 = L_1 = L_2 = L$  throughout. Compared with the  $q$ -state clock model,  $(0,0)$  is added as a possible value of the field variable. In our simulation program, we store the field variables by using labels  $m = 0, 1, 2, \dots, q$ . We assign

$$\vec{s}(0) = (0, 0) \quad (6)$$

and for  $m > 0$

$$\vec{s}(m) = (\cos(2\pi m/q), \sin(2\pi m/q)). \quad (7)$$

The reduced Hamiltonian is given by

$$\mathcal{H} = -\beta \sum_{\langle xy \rangle} \vec{s}_x \cdot \vec{s}_y - D \sum_x \vec{s}_x^2 - \vec{H} \sum_x \vec{s}_x. \quad (8)$$

In our simulations, we consider a vanishing external field  $\vec{H} = \vec{0}$  throughout. We introduce the weight factor

$$w(\vec{s}_x) = \delta_{0, \vec{s}_x^2} + \frac{1}{q} \delta_{1, \vec{s}_x^2} = \delta_{0, m_x} + \frac{1}{q} \sum_{n=1}^q \delta_{n, m_x} \quad (9)$$

that gives equal weight to  $(0,0)$  and the collection of all values  $|\vec{s}_x| = 1$ . Now the partition function can be written as

$$Z = \sum_{\{\vec{s}\}} \prod_x w(\vec{s}_x) \exp(-\mathcal{H}), \quad (10)$$

where  $\{\vec{s}\}$  denotes a configuration of the field.

Note that in the limit  $q \rightarrow \infty$ , we recover the dynamically diluted XY (ddXY) model studied in Refs. [20,21]. The reduced Hamiltonian of the ddXY model has the same form as

Eq. (8):

$$\mathcal{H}_{\text{ddXY}} = -\beta \sum_{\langle xy \rangle} \vec{\phi}_x \cdot \vec{\phi}_y - D \sum_x \vec{\phi}_x^2 - \bar{H} \sum_x \vec{\phi}_x, \quad (11)$$

where  $\vec{\phi}_x$  is a vector with two real components. The partition function is given by

$$Z = \prod_x \left[ \int d\mu(\phi_x) \right] \exp(-\mathcal{H}_{\text{ddXY}}), \quad (12)$$

with the local measure

$$d\mu(\phi_x) = d\phi_x^{(1)} d\phi_x^{(2)} \left[ \delta(\phi_x^{(1)}) \delta(\phi_x^{(2)}) + \frac{1}{2\pi} \delta(1 - |\vec{\phi}_x|) \right]. \quad (13)$$

In Ref. [14] we simulated the model with  $q = 8$ . We find  $D^* = 1.058(13)$ ; see Eq. (63) of [14]. For nearby values of  $D$ , we obtain

$$\beta_c(D = 1.05) = 0.560\,823\,90(10), \quad (14)$$

$$\beta_c(D = 1.07) = 0.558\,883\,40(10). \quad (15)$$

In Appendix B 2 of Ref. [14], we study the  $q$ -dependence of nonuniversal quantities such as the critical temperature. We find that already for  $q = 8$  the estimates differ only slightly from those for the limit  $q \rightarrow \infty$ . At the level of our statistical accuracy, estimates for  $q \geq 10$  cannot be distinguished from those for the limit  $q \rightarrow \infty$ . Taking the results of Appendix B 2 of Ref. [14], we arrive at

$$\beta_c(D = 1.05) = 0.560\,824\,18(10)[10], \quad (16)$$

$$\beta_c(D = 1.07) = 0.558\,883\,68(10)[10] \quad (17)$$

for  $q \geq 10$ . The number in square brackets gives the uncertainty of the extrapolation. The major part of the simulations here is performed for  $q = 32$ . In this case, six bits are needed to store the field variable at one site. Also, the arrays needed to store possible changes in the weight that are used to speed up the METROPOLIS and cluster updates are still small enough to fit into the cache of the CPU. We use a hybrid of local METROPOLIS and single-cluster updates [24] to simulate the model. For a detailed discussion, see Sec. IV of Ref. [14].

### III. THE OBSERVABLES

Let us define the observables measured on the finite lattice. Note that in our measurements, following Ref. [9] we replace the field at the site  $x$  by the sum of its six nearest neighbors. The idea is that statistical noise is reduced, and furthermore in the case of the  $(q + 1)$ -state clock model the rotational invariance is better approximated.

Let us define the correlation functions that are measured in the simulations. To this end, we use the notation of the  $O(N)$ -invariant  $\phi^4$  model. In the following, we denote the components of the field variable  $\vec{\phi}_x$  by  $\phi_{x,i}$  with  $i \in \{0, 1, \dots, N - 1\}$ . We study correlation functions of  $\phi$  and the two derived quantities  $s$  and  $t$ . The observables are defined for  $N \geq 2$ . In our numerical study discussed below, we consider

the case  $N = 2$ . The scalar  $s$  with charge 0 is given by

$$s_x = \sum_i \phi_{x,i} \phi_{x,i} - \bar{s}, \quad (18)$$

where  $\bar{s} = \langle \sum_i \phi_{x,i} \phi_{x,i} \rangle$  for the given lattice size. The scalar with charge 2 is given by the traceless compound

$$t_{x,ij} = \phi_{x,i} \phi_{x,j} - \delta_{ij} \frac{\phi_x^2}{N}. \quad (19)$$

Note that these lattice quantities also contain scaling fields with the same symmetry properties but larger scaling dimensions than the lowest. Furthermore, conformal invariance is only well approximated at length scales considerably larger than the lattice spacing. Therefore, the correlation functions show corrections at small distances. In the case of improved models, the leading correction should be related with the breaking of the rotational invariance of the continuum by the lattice. The corresponding correction exponent is  $\omega_r = 2.02(1)$  [20,21,25]. For a recent discussion of corrections to scaling in an improved model, see Sec. III of Ref. [14].

The two-point functions, without any normalization, are

$$g_{\phi\phi}(x_1, x_2) = \sum_i \langle \phi_{x_1,i} \phi_{x_2,i} \rangle, \quad (20)$$

$$g_{ss}(x_1, x_2) = \langle s_{x_1} s_{x_2} \rangle, \quad (21)$$

$$g_{tt}(x_1, x_2) = \sum_{ik} \langle t_{x_1,i,k} t_{x_2,i,k} \rangle. \quad (22)$$

We consider the following three-point correlation functions:

$$G_{\phi\phi s}(x_1, x_2, x_3) = \sum_i \langle \phi_{x_1,i} \phi_{x_2,i} s_{x_3} \rangle, \quad (23)$$

$$G_{sss}(x_1, x_2, x_3) = \langle s_{x_1} s_{x_2} s_{x_3} \rangle, \quad (24)$$

$$G_{tt s}(x_1, x_2, x_3) = \sum_{ik} \langle t_{x_1,i,k} t_{x_2,i,k} s_{x_3} \rangle, \quad (25)$$

$$G_{\phi\phi t}(x_1, x_2, x_3) = \sum_{ik} \langle \phi_{x_1,i} \phi_{x_2,k} t_{x_3,i,k} \rangle. \quad (26)$$

Note that our normalizations of the two- and three-point functions are not the same as those of Refs. [3,5]. This leads to a factor of  $\sqrt{2}$  in the result for  $\lambda_{\phi\phi t}$ , while it cancels in the other three cases [26].

#### A. Our choices for $x_1, x_2$ , and $x_3$

The variance reduction method requires that the lattice is subdivided into blocks. For technical reasons, we compute correlation functions only for the sites at the center of these blocks. These sites are given by  $x^{(i)} = n_s k_i$ . In our simulations, we have used the three different choices  $n_s = 2, 4$ , and  $6$ . Throughout the linear lattice size  $L$  is a multiple of  $n_s$  and  $k_i \in \{0, 1, \dots, L/n_s - 1\}$ . In the following, we refer to  $n_s$  as stride. To keep the study tractable, we have to single out a few directions for the displacements between the points. In the case of the two-point functions, we consider displacements along the axes, the face diagonals, and the space diagonals. In the following, these are indicated by (a), (f), and (d), respectively. In our simulation program, we summed over all choices that are related by symmetry to reduce the statistical

error. In the following, we shall denote the two-point function by  $g_{r,O_1,O_2}(x)$ , where  $r \in \{a, f, d\}$  gives the direction and  $x = |x_1 - x_2|$  is the distance between the two points. In the case of the three-point functions

$$G_{r,O_1,O_2,O_3}(x) = \langle O_1(x_1)O_2(x_2)O_3(x_3) \rangle, \quad (27)$$

we consider two different geometries that are indicated by  $r$ . For  $r = f$ , the largest displacement is along a face diagonal. For example,

$$x_3 - x_1 = (j, 0, 0), \quad x_3 - x_2 = (0, j, 0). \quad (28)$$

Our second choice is indicated by  $r = d$  and the largest displacement is along a space diagonal. For example,

$$x_3 - x_1 = (j, 0, 0), \quad x_3 - x_2 = (0, j, j), \quad (29)$$

where  $j = n_s k$ , where  $k$  is an integer. Also here we sum in our simulation over all choices that are related by symmetry to reduce the statistical error. The argument  $x$  of  $G$  gives the smallest distance between two points  $x = j$ .

To eliminate the constants  $C_i$ , Eq. (1), and the power-law behavior from the three-point functions, we directly normalized our estimates of the three-point functions by the corresponding ones of two-point functions. For the direction  $r = f$  we get, for example,

$$\lambda_{\phi\phi t} \simeq 2^{-\Delta_t/2} \frac{G_{f,\phi\phi t}(x)}{g_{a,\phi\phi}(x) g_{f,tt}^{1/2}(\sqrt{2}x)}. \quad (30)$$

Based on the numbers given in Table I, we used as numerical values  $\Delta_t = 1.23629$ ,  $\Delta_s = 1.5113$ , and  $\Delta_\phi = 0.51908$  for the scaling dimensions. Note that the systematic error of the estimate of  $\lambda_{ijk}$  due to the uncertainty of the scaling dimensions is negligible.

## B. Variance reduced measurement

The variance reduction method used here is based on the ideas of Refs. [11,12]. The method is discussed in detail in Sec. V of Ref. [9]. Here we summarize the basics for completeness.

In the case of an  $N$ -point correlation function, the lattice is partitioned into  $N$  areas  $B_i$ , where each of these areas contains one of the sites  $x_1, x_2, \dots, x_N$ . These areas are chosen such that for each pair  $i \neq j$  none of the sites in  $B_i$  is a nearest neighbor of a site in  $B_j$ . Let us denote the collection of the remaining sites as  $R$ . Now the sampling of the correlation function can be reorganized in the following way.

In a straightforward approach, one would estimate the expectation value of the  $N$ -point correlation function by averaging over  $M$  configurations,

$$\begin{aligned} & \overline{O_1(x_1)O_2(x_2) \cdots O_N(x_N)} \\ &= \frac{1}{M} \sum_{\alpha} O_{1,\alpha}(x_1)O_{2,\alpha}(x_2) \cdots O_{N,\alpha}(x_N), \end{aligned} \quad (31)$$

where  $\alpha$  labels configurations that have been generated by using a Markov chain. We assume that the process is equilibrated and the configurations are generated with a probability density proportional to the Boltzmann factor.  $O_{i,\alpha}(x_i)$  denotes the value of  $O_i(x_i)$  assumed for configuration  $\alpha$ .

In the case of the variance reduced measurement, we first average  $O_i(x_i)$  over configurations on  $B_i$  that have been generated while keeping the field on  $R$  fixed:

$$\begin{aligned} & \overline{O_1(x_1)O_2(x_2) \cdots O_N(x_N)} \\ &= \frac{1}{M} \sum_{\alpha} \overline{O_{1,\alpha}(x_1)} \overline{O_{2,\alpha}(x_2)} \cdots \overline{O_{N,\alpha}(x_N)}, \end{aligned} \quad (32)$$

where

$$\overline{O_{i,\alpha}(x_i)} = \frac{1}{m} \sum_{\gamma} O_{i,\alpha,\gamma}(x_i). \quad (33)$$

Here we have generated  $m$  configurations labeled by  $\gamma$  on  $B_i$ , keeping the field on  $R$  fixed. The configurations on  $R$  are labeled by  $\alpha$ . The effect of this averaging for each site separately is that we consider  $m^N$  configurations for the  $N$ -point function. For small  $m$ , this translates into

$$\epsilon^2 \propto \frac{1}{m^N} \quad (34)$$

for the statistical error  $\epsilon$  of the estimate of the  $N$ -point correlation function. As  $m$  increases, the effect of fixing the configuration on  $R$  becomes visible and  $\epsilon^2$  converges to a finite limit as  $m \rightarrow \infty$  and can be reduced only by increasing  $M$ . There is in general an optimal value of  $m$ . This value of  $m$  depends on the choice of  $O_i$  and the distances. Finding a good choice of  $m$  requires some numerical experimentation. Below we shall specify our implementation of this general idea.

We only used the sites  $(j_0 n_s, j_1 n_s, j_2 n_s)$ , with  $j_i \in \{0, n_s, 2n_s, \dots, L_i/n_s - 1\}$  for the measurements of the two- and three-point functions. As areas we consider blocks of the size  $l_b^3$ , where  $l_b = 2n_s - 1$ . The sites used for the measurement are at the center of the blocks.

Computing the block averages, we used local updates only. In particular, in the case of the  $(q+1)$ -clock model, we used the first version of the METROPOLIS update discussed in Sec. IV A of Ref. [14]. Computing averages for the blocks, keeping the remainder  $R$  fixed, we update more frequently toward the center of the blocks. To this end, we perform a cycle of updates, similar to the cycle used in a multigrid updating scheme. In particular, we sweep over subblocks of the size  $3^3, 5^3, \dots, l_b^3$ . In addition, as the smallest subset, we consider the central site and its six nearest neighbors. For each of these sweeps, we perform a measurement. The frequency  $n_x$  of the sweeps is chosen such that the number of sites times  $n_x$  is roughly the same for all sizes. For example, in the case  $n_s = 6$ , where  $l_b = 11$ , in one such cycle 268 measurements are performed. In our production runs for  $n_s = 6$ , we performed 160 update cycles for a given configuration on the remainder  $R$ . Hence in total  $160 \times 268 = 42\,880$  measurements are performed for a given configuration on  $R$ .

Note that for our setup, two blocks with the central sites  $x_1$  and  $x_2$  are separated if  $|x_1^{(i)} - x_2^{(i)}| \geq 2n_s$  for at least one direction  $i$ . Computing the two- and three-point functions, one therefore has to note that only results for  $|x_k^{(i)} - x_l^{(i)}| \geq 2n_s$  for at least one direction  $i$  are valid.

The simulation is built up in the following way: First we equilibrate the system without measuring by performing 2000 times the following sequence of updates: one sweep with the METROPOLIS update type 2, one sweep with the METROPOLIS



update type 1, and  $L$  times a single cluster update. These updates are discussed in Sec. IV of Ref. [14].

For each measurement, we performed ten times the following sequence of updates: two METROPOLIS sweeps followed by  $L$  single cluster updates. In the first and the sixth sequence, the first METROPOLIS is of type 2, while all others are of type 1. Note that here the measurements, including the updates of the blocks for variance reduction, are far more expensive than the updates of the system as a whole. Therefore, between the measurements, a relatively large number of updates is performed in order to measure on essentially uncorrelated configurations. In principle, the final configurations of separated blocks could be used as an update of the main Markov chain. In our case, a  $1/2^3$  of the blocks could be used to this end. For simplicity, we abstained from doing so.

### C. Finite-size effects

Compared with the linear size  $L$  of the lattice, the distances that we consider for our two- and three-point functions are small. In that respect, they can be viewed as local scalar operators with charge 0 such as the energy density. The energy density on a finite lattice of the linear size  $L$ , for a vanishing external field, behaves as

$$E(\beta_c, L) = cL^{-\Delta_s} + E_{\text{ns}}. \quad (35)$$

For a discussion, see Sec. IV of Ref. [9]. In the analysis of our data, we assume that the finite-size scaling behavior of the two- and three-point functions is given by Eq. (35), where, of course, the values of the constants depend on the quantity that is considered. Given the huge amount of data, we abstain from sophisticated fitting with *Ansätze* motivated by Eq. (35). Instead, we consider pairs of linear lattice sizes  $L_1 = L$ ,  $L_2 = 2L$ , and we compute

$$G_{\text{ex}}(2L) := G(2L) + \frac{G(2L) - G(L)}{2^{\Delta_s} - 1}, \quad (36)$$

where  $G$  is the quantity under consideration. Equation (36) is derived by inserting  $L_1$  and  $L_2$  into Eq. (35) and solving the system of two equations with respect to the nonsingular (ns) part that remains in the limit  $L \rightarrow \infty$ . As in the case of Eq. (30), we use  $\Delta_s = 1.5113$  as the numerical value for the scaling dimension. In the analysis of the numerical data, for simplicity, we apply Eq. (36) to our estimates of the scaling dimension and the OPE coefficients  $\lambda_{ijk}$  computed for finite lattice sizes  $L$ . Note that the first term on the right-hand side of Eq. (35) is subject to corrections to scaling. Given the small number of different linear lattice sizes  $L$  that we consider here, these are not taken into account in the extrapolation. Their effect is monitored by comparing the results obtained by using different values of  $L$  in the extrapolation.

## IV. NUMERICAL RESULTS

### A. Preliminary simulations

To check the  $q$ -dependence of our results for the  $(q+1)$ -state clock model, we have simulated the linear lattice size  $L = 120$  with stride  $n_s = 2$  for  $q = 8, 16$ , and  $32$ . In all three cases,  $D = 1.05$ . In the case of  $q = 8$ , we simulated at  $\beta = 0.56082390$ , Eq. (14), and for  $q = 16$  and  $32$  at  $\beta$

$= 0.56082418$ , Eq. (16). The statistics is 139 100, 139 640, and 259 820 measurements, respectively. For each measurement, we performed  $m = 40$  measurements on the blocks. For each block measurement, we performed one sweep over the  $3^3$  blocks. We compared the results for the four different OPE coefficients for all distances studied. At the level of our statistical accuracy, we find no dependence on  $q$ . Therefore, we are confident that the results obtained below for  $q = 32$  are essentially unaffected by the breaking of the  $O(2)$ -symmetry.

Furthermore, we simulated the  $O(2)$ -symmetric  $\phi^4$ -model at  $\lambda = 2.1$  and  $\beta = 0.5091504$ , Eq. (4). We simulated the linear lattice size  $L = 120$  and used the stride  $n_s = 2$ . We performed 81 970 measurements with  $m = 60$  updates of the blocks for each measurement. We compared our results for the OPE coefficients with those for the  $(q+1)$ -state clock model discussed above. In particular, comparing with the  $q = 32$  case, we only find a difference that is clearly out of the error bars for  $\lambda_{\text{SSS}}$  at the distance  $x = 4$ . In the case of the  $\phi^4$  model, we get 0.87927(40) and 0.84335(64) for the directions  $f$  and  $d$ , respectively. These numbers can be compared with 0.87698(30) and 0.84026(49) for the  $(32+1)$ -state clock model. We also simulated the  $\phi^4$ -model for the stride  $n_s = 4$  and the linear lattice size  $L = 240$ . Here we find no difference compared with the corresponding simulations of the  $(32+1)$ -state clock model discussed below. Hence the small distance effects in the correlation functions are mainly caused by the lattice and the nearest-neighbor interaction.

Since the simulation of the  $\phi^4$  model takes about three times as much CPU time as that of the  $(q+1)$ -state clock model [14] and 16 times as much memory is needed to store the configurations, we simulated the  $(q+1)$ -state clock model with  $q = 32$  in the major part of our study.

### B. Production runs using the $(32+1)$ -state clock model

In the major part of our study, we simulated the  $(32+1)$ -state clock model with the linear lattice sizes  $L = 240, 480$ , and  $960$ . We performed measurements by using the strides  $n_s = 2, 4$ , and  $6$ . In principle, one could do the measurements for these three different strides in the same set of simulations. However, for simplicity, for a given simulation we performed measurements for one value of  $n_s$  only.

Our final results are mainly based on the simulations with  $n_s = 6$ . For  $n_s = 6$ , we performed 70 587, 11 196, and 1272 update and measurement cycles for  $L = 240, 480$ , and  $960$ , respectively. On one core of an AMD EPYC 7351P 16-Core Processor, the simulations using  $n_s = 6$  took about 10 years in total.

### C. Scaling dimensions from the two-point correlation functions

As a check, we extract the scaling dimensions  $\Delta_\phi$ ,  $\Delta_s$ , and  $\Delta_t$  from the behavior of the two-point functions  $g(x)$ . In the first step, we compute

$$\Delta_{\text{eff}}(x, \Delta x) = -\frac{1}{2} \frac{\ln[g(x + \Delta x)/g(x)]}{\ln[(x + \Delta x)/x]}, \quad (37)$$

where  $\Delta x = n_s$ ,  $\Delta x = \sqrt{2}n_s$ , and  $\Delta x = \sqrt{3}n_s$  for  $r = a, f$ , and  $d$ , respectively. These results are extrapolated to the infinite volume by using Eq. (36).

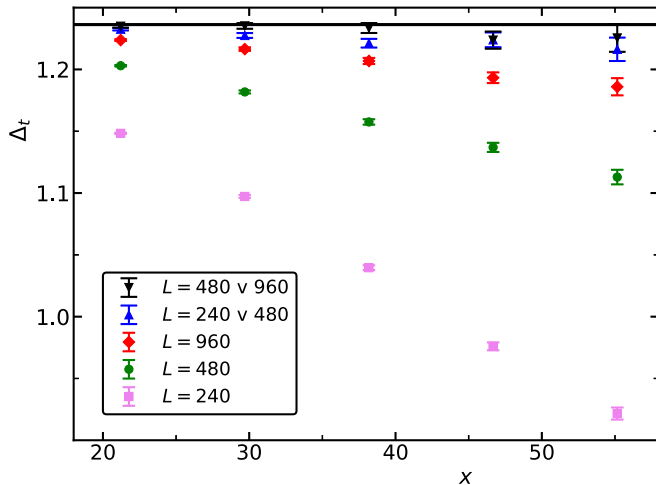


FIG. 1. We plot our numerical estimates of  $\Delta_t$  as a function of the distance  $x$  between the lattice sites. Here we plot results for the direction  $f$  only. The stride is  $n_s = 6$  throughout. We give estimates computed for the linear lattice sizes  $L = 240, 480$ , and  $960$  and the extrapolations using the pairs  $(240, 480)$  and  $(480, 960)$  of linear lattice sizes. For comparison, we give the estimate obtained by using the conformal bootstrap method [5] as a solid black line.

In Fig. 1 we demonstrate the effectiveness of the extrapolation. We give the results for  $\Delta_t$  obtained for the linear lattice sizes  $L = 240, 480$ , and  $960$ . The measurements are performed with the stride  $n_s = 6$ . Here we give results for the direction  $f$  only. We see a clear dependence of the results on  $L$  that increases with increasing distance. In contrast, the extrapolated results for  $(L_1, L_2) = (240, 480)$  and  $(L_1, L_2) = (480, 960)$  differ only slightly. Note that the error bars given in Fig. 1, as for the figures below, are purely statistical, indicating one standard deviation. Furthermore, for a given  $n_s$ , the results for different distances are obtained from the same simulations. Hence there is a statistical cross-correlation.

Next we check for the effect of operators with higher dimension in the same channel. The effect should decay with increasing distance between the two sites. In Fig. 2 we plot extrapolated results for  $(L_1, L_2) = (480, 960)$  of  $\Delta_t$ . Data are taken from our runs for the strides  $n_s = 2$  and  $6$ . We give results for all three directions that we consider. Similar to the case of the Blume-Capel model on the simple-cubic lattice, we find that the amplitude of corrections is quite different for different directions [9]. For the direction  $f$  the deviations at small distances  $x$  are the smallest, while for  $d$  they are the largest. To check whether it is plausible that corrections due to the violation of rotational symmetry by the lattice dominate, as discussed in Sec. III above, we plot  $D + cx^{-2.02}$  as dashed and dash-dotted lines for the directions  $a$  and  $d$ , respectively. For  $D$  we take the value of  $\Delta_t$  obtained by the CB method. The coefficient  $c$  is simply chosen such that the numerical estimate of  $\Delta_t$  at  $x = 8$  and  $6 \times \sqrt{3}$  for the directions  $a$  and  $d$  are matched, respectively.

The observations are similar for  $\Delta_s$  and  $\Delta_\phi$ , so we do not discuss them in detail here. Our numerical result for  $\Delta_t$  is consistent with that obtained by using the CB method [5] and previous Monte Carlo simulations. However, we do not reach the accuracy of [5] and the lattice result [15]. As

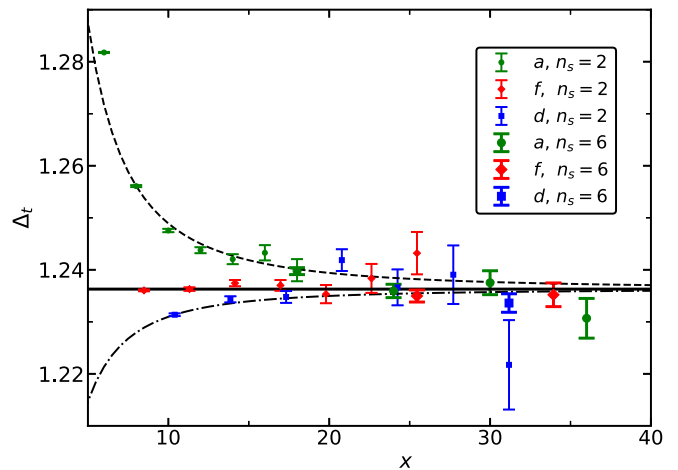


FIG. 2. We plot  $\Delta_t$  obtained by extrapolating our results for  $(L_1, L_2) = (480, 960)$  as a function of the distance  $x$  between the lattice sites. These results are obtained by using the strides  $n_s = 2$  and  $6$ . We omit the results for  $n_s = 4$  to keep the figure readable.  $a$ ,  $f$ , and  $d$  denote the three different directions that we consider. For comparison, we give the estimate obtained by using the conformal bootstrap method [5] as a solid black line. In addition, we give dashed and dash-dotted lines that include an estimate of corrections to scaling for the directions  $a$  and  $d$ , respectively. For a discussion, see the text.

our final estimate, we might quote  $\Delta_t = 1.2352(23)$  from the extrapolation of  $(L_1, L_2) = (480, 960)$  for the direction  $f$  and the pair of distances  $(12, 18) \times \sqrt{2}$ . Looking at Figs. 1 and 2 it seems plausible that for this choice, systematic errors due to the finite value of  $x$  and due to the imperfection of the extrapolation to the infinite volume are not larger than the statistical error.

In a similar way we get  $\Delta_\phi = 0.51953(32)$  from the extrapolation of  $(L_1, L_2) = (480, 960)$ , the stride  $n_s = 2$ , the direction  $f$ , and the pair of distances  $(12, 14) \times \sqrt{2}$ , or  $\Delta_\phi = 0.51864(52)$  for the stride  $n_s = 6$  and the pair of distances  $(12, 18) \times \sqrt{2}$ . Finally, we obtain from the measurements with the stride  $n_s = 6$ , the direction  $f$ , and the pair of distances  $(12, 18) \times \sqrt{2}$  the estimate  $\Delta_s = 1.5098(21)$ .

#### D. OPE coefficients and the three-point functions

Here we follow a similar procedure to that for the scaling dimensions. In the first step, we compute estimates of  $\lambda_{ijk}$  for given linear lattice sizes  $L$  by using Eq. (30) and analogous equations. Then we extrapolate to the infinite volume by using Eq. (36). Similar to Ref. [9], we have measured the three-point function for two different geometries that we denote by  $f$  and  $d$ . It turns out that small distance corrections are smaller for  $f$ . Final results, however, are fully consistent. Therefore, in the following we restrict the detailed discussion on geometry  $f$ .

In Fig. 3 we plot results for  $\lambda_{\phi\phi_s}$  obtained from simulations with the stride  $n_s = 6$  and the linear lattice sizes  $L = 240, 480$ , and  $960$ . In addition, we give the results of the extrapolation using Eq. (36) and the pairs of lattice sizes  $(L_1, L_2) = (240, 480)$  and  $(L_1, L_2) = (480, 960)$ . We see a clear dependence of the results on  $L$  that increases with increasing distance  $x$ . In contrast, the extrapolated results for

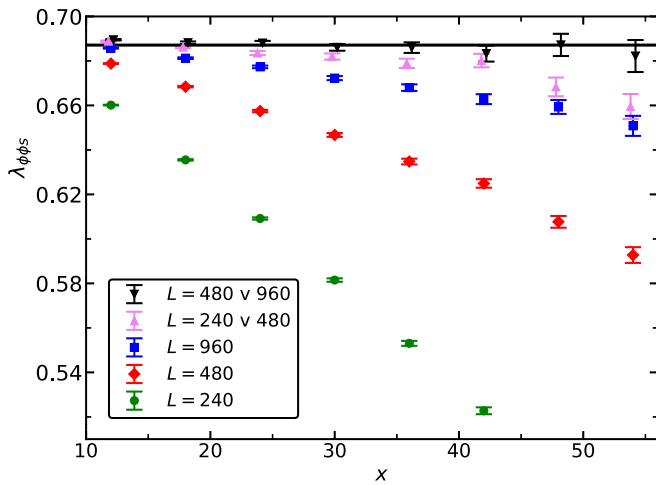


FIG. 3. We plot our numerical results for  $\lambda_{\phi fs}$  as a function of the distance  $x$ . Here we consider simulations with stride  $n_s = 6$  and three-point functions for the geometry  $f$ . We give results for the linear lattice sizes  $L = 240, 480$ , and  $960$ . These results are extrapolated by using Eq. (36) for the pairs  $(240, 480)$  and  $(480, 960)$  of linear lattice sizes. The distance  $x$  for the pair  $(240, 480)$  is slightly shifted to make the figure more readable. For comparison, we give the estimate obtained by using the conformal bootstrap method [5] as a solid black line.

$(L_1, L_2) = (240, 480)$  and  $(L_1, L_2) = (480, 960)$  differ only slightly. Only for distances  $x \geq 48$  does the estimate obtained from the pair  $(L_1, L_2) = (240, 480)$  decrease significantly with increasing distance  $x$ . Based on this observation, we conclude that the extrapolation for  $(L_1, L_2) = (480, 960)$  is reliable in the range of distances  $x$  considered below. We have

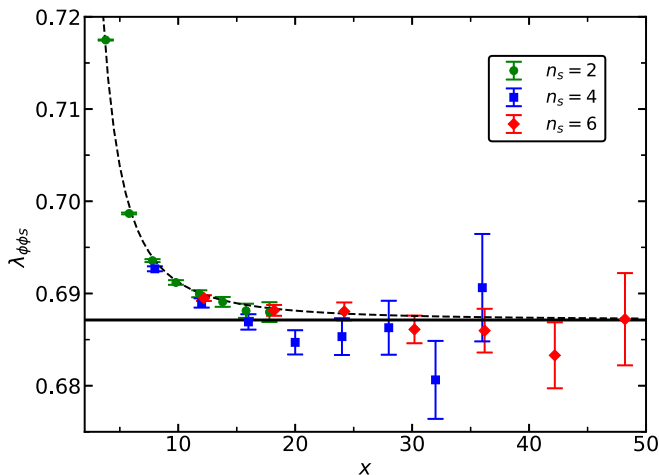


FIG. 4. We plot our numerical results for  $\lambda_{\phi fs}$  as a function of the distance between the lattice sites. Here we consider simulations with stride  $n_s = 2, 4$ , and  $6$ , and three-point functions for the geometry  $f$ . We give results for the extrapolation of the lattice sizes  $(L_1, L_2) = (480, 960)$ . The values of  $x$  for  $n_s = 2$  and  $6$  are slightly shifted to reduce the overlap of the symbols. For comparison, we give the estimate obtained by using the conformal bootstrap method [5] as a solid black line. The dashed line contains in addition a correction  $\propto x^{-2.02}$ .

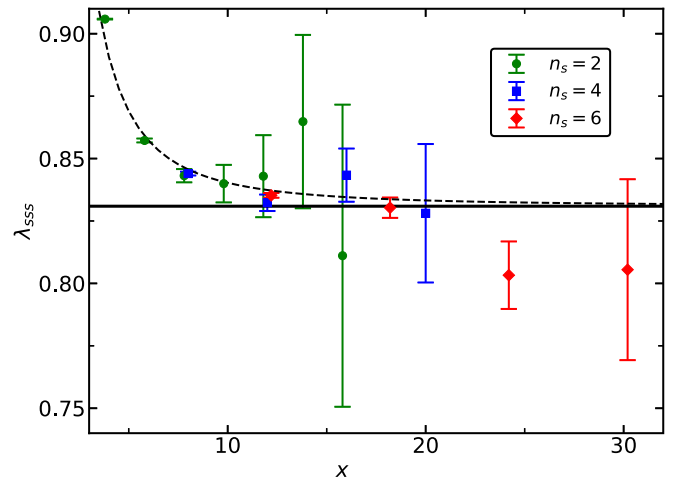


FIG. 5. We plot our numerical results for  $\lambda_{s ss}$  as a function of the distance between the lattice sites. Here we consider simulations with stride  $n_s = 2, 4$ , and  $6$ , and three-point functions for the geometry  $f$ . We give results for the extrapolation of the lattice sizes  $L = 480$  and  $960$ . The values of  $x$  for  $n_s = 2$  and  $6$  are slightly shifted to reduce the overlap of the symbols. For comparison, we give the estimate obtained by using the conformal bootstrap method [5] as a solid black line. The dashed line contains in addition a correction  $\propto x^{-2.02}$ .

checked that the same also holds for the other three OPE coefficients that we study.

Next, in Fig. 4 we plot the extrapolated results for  $(L_1, L_2) = (480, 960)$  obtained for the strides  $n_s = 2, 4$ , and  $6$ . To check whether it is plausible that corrections due to the violation of rotational symmetry by the lattice dominate, we plot  $l + cx^{-2.02}$  as a dashed line, where  $l$  is the estimate of  $\lambda_{\phi fs}$  obtained by the CB method and  $c$  is chosen such that our

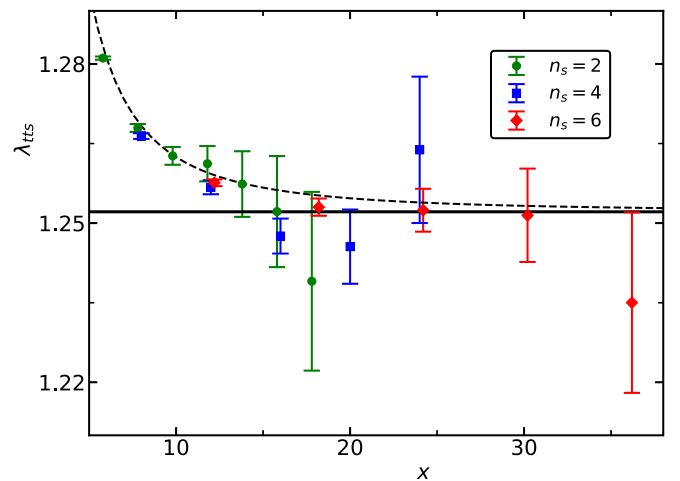


FIG. 6. We plot our numerical results for  $\lambda_{t ts}$  as a function of the distance  $x$  between the lattice sites. Here we consider simulations with stride  $n_s = 2, 4$ , and  $6$ , and three-point functions for the geometry  $f$ . We give results for the extrapolation of the lattice sizes  $L = 480$  and  $960$ . The values of  $x$  for  $n_s = 2$  and  $6$  are slightly shifted to reduce the overlap of the symbols. For comparison, we give the estimate obtained by using the conformal bootstrap method [5] as a solid black line. The dashed line contains in addition a correction  $\propto x^{-2.02}$ .

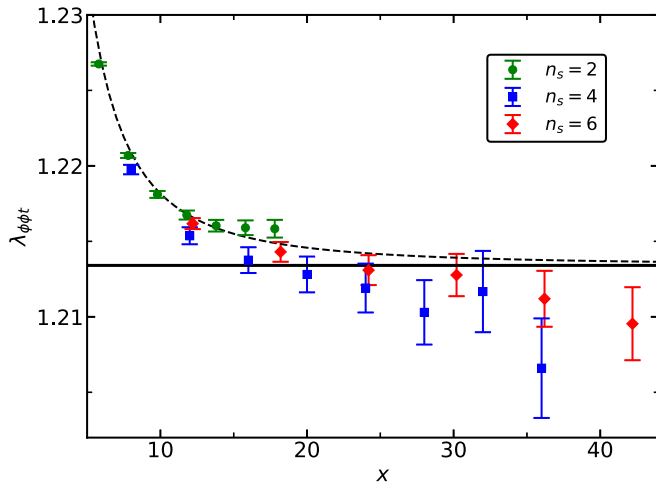


FIG. 7. We plot our numerical results for  $\lambda_{\phi\phi t}$  as a function of the distance between the lattice sites. Here we consider simulations with stride  $n_s = 2, 4$ , and  $6$ , and three-point functions for the geometry  $f$ . We give results for the extrapolation of the lattice sizes  $L = 480$  and  $960$ . The values of  $x$  for  $n_s = 2$  and  $6$  are slightly shifted to reduce the overlap of the symbols. For comparison, we give the estimate obtained by using the conformal bootstrap method [5] as a solid black line. The dashed line contains in addition a correction  $\propto x^{-2.02}$ . Note that we have multiplied our numbers, which are based on Eqs. (20), (22), and (26), by a factor of  $\sqrt{2}$  to match with the conventions of Ref. [5].

numerical estimate for the distance  $x = 6$  is matched. Indeed, the data fall reasonably well on the dashed line. In the case of  $n_s = 4$  and  $x = 20$  there is a deviation by about 2.6 standard deviations. The deviations at  $x = 12$  and  $16$  go in the same direction. Since the estimates at different distances are obtained from the same simulations, there is a statistical correlation between them. Hence it is still reasonable to attribute these deviations to statistical fluctuations. For the stride  $n_s = 6$  we get  $\lambda_{\phi\phi s} = 0.6881(10)$  at  $x = 24$ . The dashed line suggests that for  $x = 24$  the finite  $x$  effect is smaller than the statistical error. Hence one might base a final result on this estimate.

Next let us discuss the numerical results for  $\lambda_{sss}$ . First we convinced ourselves that also here the extrapolation using Eq. (36) is effective. In Fig. 5 we give results of the extrapolation using the linear lattice sizes  $L = 480$  and  $960$  for the strides  $n_s = 2, 4$ , and  $6$ . The relative statistical error is larger than for  $\lambda_{\phi\phi s}$ . The effect of the variance reduction is more important than for  $\lambda_{\phi\phi s}$ . Going to larger distances, it is mandatory to use larger block sizes.

Similar to Fig. 4, we plot  $l + cx^{-2.02}$  as a dashed line, where  $l$  is the estimate of  $\lambda_{sss}$  obtained by the CB method, and  $c$  is chosen such that our numerical estimate for the distance

$x = 6$  is matched. Based on that, it seems plausible that for the stride  $n_s = 6$  at the distance  $x = 18$ , the small distance error is at most of a similar size to the statistical one. We read off  $\lambda_{sss} = 0.8303(41)$ .

Next, in Fig. 6 we plot our extrapolated results for  $\lambda_{tts}$  obtained from the simulations with the strides  $n_s = 2, 4$ , and  $6$ . Similar to Fig. 4, we plot  $l + cx^{-2.02}$  as a dashed line, where  $l$  is the estimate of  $\lambda_{tts}$  obtained by the CB method, and  $c$  is chosen such that our numerical estimate for the distance  $x = 6$  is matched. The final result could be based on the estimate  $\lambda_{tts} = 1.2530(16)$  obtained by using the stride  $n_s = 6$  at the distance  $x = 18$ .

Finally, in Fig. 7 we plot our numerical results for  $\lambda_{\phi\phi t}$ . Similar to Fig. 4, we plot  $l + cx^{-2.02}$  as a dashed line, where  $l$  is the estimate of  $\lambda_{\phi\phi t}$  obtained by the CB method and  $c$  is chosen such that our numerical estimate for the distance  $x = 6$  is matched.

We read off  $\lambda_{\phi\phi t} = 1.214(7)$  for  $x = 18$  and the stride  $n_s = 6$ . For the distance  $x = 24$ , we get  $\lambda_{\phi\phi t} = 1.213(10)$  instead. Note that we have multiplied our numbers, which are based on Eqs. (20), (22), and (26), by a factor of  $\sqrt{2}$  to match with the conventions of Ref. [5].

## V. SUMMARY AND DISCUSSION

We have demonstrated that OPE coefficients for the three-dimensional XY universality class can be determined by using Monte Carlo simulations of a lattice model with a relative error of about 1% or less. To this end, we have simulated the improved  $(32 + 1)$ -state clock model using linear lattice sizes up to  $L = 960$ . The outline of the study is similar to that of Ref. [9], where we studied the Ising universality class. The key ideas are variance reduced estimators of the two- and three-point correlation function and an extrapolation to the infinite volume.

Our results are fully consistent with those recently obtained by using the conformal bootstrap (CB) method [5], further confirming that the CB method and the lattice model examine the same RG fixed point. One has to note, however, that the estimates obtained by using the CB method are by about two orders of magnitude more precise than those obtained here.

There is still room for improvement. For example, the measurement, which takes considerably more CPU time than the generation of the configurations, could be easily parallelized and could hence be speeded up, for example by running it on graphics processing units.

## ACKNOWLEDGMENT

This work was supported by the Deutsche Forschungsgemeinschaft (DFG) under Grant No. HA 3150/5-1.

[1] D. Simmons-Duffin, *The Conformal Bootstrap. Proceedings, Theoretical Advanced Study Institute in Elementary Particle Physics: New Frontiers in Fields and Strings* (TASI, Boulder, CO, 2015).

[2] D. Poland, S. Rychkov, and A. Vichi, The conformal bootstrap: Theory, numerical techniques, and applications, *Rev. Mod. Phys.* **91**, 015002 (2019).



- [3] F. Kos, D. Poland, D. Simmons-Duffin, and A. Vichi, Precision islands in the Ising and  $O(N)$  models, *J. High Energy Phys.* **08** (2016) 036.
- [4] D. Simmons-Duffin, The lightcone bootstrap and the spectrum of the 3d Ising CFT, *J. High Energy Phys.* **03** (2017) 086.
- [5] S. M. Chester, W. Landry, J. Liu, D. Poland, D. Simmons-Duffin, N. Su, and A. Vichi, Carving out OPE space and precise  $O(2)$  model critical exponents, *J. High Energy Phys.* **06** (2020) 142.
- [6] M. Caselle, G. Costagliola, and N. Magnoli, Numerical determination of the operator-product-expansion coefficients in the 3D Ising model from off-critical correlators, *Phys. Rev. D* **91**, 061901 (2015).
- [7] G. Costagliola, Operator product expansion coefficients of the 3D Ising model with a trapping potential, *Phys. Rev. D* **93**, 066008 (2016).
- [8] V. Herdeiro, Numerical estimation of structure constants in the three-dimensional Ising conformal field theory through Markov chain uv sampler, *Phys. Rev. E* **96**, 033301 (2017).
- [9] M. Hasenbusch, Two- and three-point functions at criticality: Monte Carlo simulations of the improved three-dimensional Blume-Capel model, *Phys. Rev. E* **97**, 012119 (2018).
- [10] A. M. Polyakov, Conformal symmetry of critical fluctuations, *Pis'ma Zh. Eksp. Teor. Fiz.* **12**, 538 (1970) [*JETP Lett.* **12**, 381 (1970)].
- [11] G. Parisi, R. Petronzio, and F. Rapuano, A measurement of the string tension near the continuum limit, *Phys. Lett. B* **128**, 418 (1983).
- [12] M. Lüscher and P. Weisz, Locality and exponential error reduction in numerical lattice gauge theory, *J. High Energy Phys.* **09** (2001) 010.
- [13] W. Xu, Y. Sun, J.-P. Lv, and Y. Deng, High-precision Monte Carlo study of several models in the three-dimensional  $U(1)$  universality class, *Phys. Rev. B* **100**, 064525 (2019).
- [14] M. Hasenbusch, Monte Carlo study of an improved clock model in three dimensions, *Phys. Rev. B* **100**, 224517 (2019).
- [15] M. Hasenbusch and E. Vicari, Anisotropic perturbations in three-dimensional  $O(N)$ -symmetric vector models, *Phys. Rev. B* **84**, 125136 (2011).
- [16] J. A. Lipa, D. R. Swanson, J. A. Nissen, T. C. P. Chui, and U. E. Israelsson, Heat Capacity and Thermal Relaxation of Bulk Helium Very Near the Lambda Point, *Phys. Rev. Lett.* **76**, 944 (1996).
- [17] J. A. Lipa, D. R. Swanson, J. A. Nissen, Z. K. Geng, P. R. Williamson, D. A. Stricker, T. C. P. Chui, U. E. Israelsson, and M. Larson, Specific Heat of Helium Confined to a 57- $\mu\text{m}$  Planar Geometry, *Phys. Rev. Lett.* **84**, 4894 (2000).
- [18] J. A. Lipa, J. A. Nissen, D. A. Stricker, D. R. Swanson, and T. C. P. Chui, Specific heat of liquid helium in zero gravity very near the  $\lambda$ -point, *Phys. Rev. B* **68**, 174518 (2003).
- [19] A. Pelissetto and E. Vicari, Critical phenomena and renormalization-group theory, *Phys. Rep.* **368**, 549 (2002).
- [20] M. Campostrini, M. Hasenbusch, A. Pelissetto, P. Rossi, and E. Vicari, Critical behavior of the three-dimensional XY universality class, *Phys. Rev. B* **63**, 214503 (2001).
- [21] M. Campostrini, M. Hasenbusch, A. Pelissetto, and E. Vicari, The critical exponents of the superfluid transition in He4, published as Theoretical estimates of the critical exponents of the superfluid transition in He4 by lattice methods, *Phys. Rev. B* **74**, 144506 (2006).
- [22] J. H. Chen, M. E. Fisher, and B. G. Nickel, Unbiased Estimation of Corrections to Scaling by Partial Differential Approximants, *Phys. Rev. Lett.* **48**, 630 (1982).
- [23] M. E. Fisher and J. H. Chen, The validity of hyperscaling in three dimensions for scalar spin systems, *J. Phys. (Paris)* **46**, 1645 (1985).
- [24] U. Wolff, Collective Monte Carlo Updating for Spin Systems, *Phys. Rev. Lett.* **62**, 361 (1989).
- [25] M. Campostrini, A. Pelissetto, P. Rossi, and E. Vicari, Two-point correlation function of three-dimensional  $O(N)$  models: The critical limit and anisotropy, *Phys. Rev. E* **57**, 184 (1998).
- [26] D. Simmons-Duffin (private communication).